

LDTR: Transformer-based Lane Detection with Anchor-chain Representation

Zhongyu Yang¹, Chen Shen², Wei Shao², Tengfei Xing², Runbo Hu², Pengfei Xu², Hua Chai², and Ruini Xue¹(✉)

© The Author(s)

Abstract Despite recent advances in lane detection methods, scenarios with limited- or no-visual-clue of lanes due to factors such as lighting conditions and occlusion remain challenging and crucial for automated driving. Moreover, current lane representations require complex post-processing and struggle with specific instances. Inspired by the DETR architecture, we propose LDTR, a transformer-based model to address these issues. Lanes are modeled with a novel anchor-chain, regarding a lane as a whole from the beginning, which enables LDTR to handle special lanes inherently. To enhance lane instance perception, LDTR incorporates a novel multi-referenced deformable attention module to distribute attention around the object. Additionally, LDTR incorporates two line IoU algorithms to improve convergence efficiency and employs a Gaussian heatmap auxiliary branch to enhance model representation capability during training. To evaluate lane detection models, we rely on Fréchet distance, parameterized F1-score, and additional synthetic metrics. Experimental results demonstrate that LDTR achieves state-of-the-art performance on well-known datasets.

Keywords Transformer, Lane detection, Anchor-chain.

1 Introduction

Autonomous driving is an important application of deep learning, in which the ability to perceive road elements is particularly crucial, especially lane markings, one of the

¹ University of Electronic Science and Technology of China, Chengdu, 611731, China. E-mail: Z. Yang, 202021080612@std.uestc.edu.cn; R. Xue, xueruini@uestc.edu.cn(✉).

² Didi Chuxing, Beijing, 100081, China. E-mail: C. Shen, jayshenchen@didiglobal.com; W. Shao, wayneshaowei@didiglobal.com; T. Xing, xingtengfei@didiglobal.com; R. Hu, hurunbo@didiglobal.com; P. Xu, pengfeixu@didiglobal.com; H. Chai, chaihua@didiglobal.com.

Manuscript received: 2024-01-18; accepted: 2024-02-29

most essential components of road traffic signs. However, due to the complexity of road scenarios and lane deformation from varying perspectives, accurate lane detection remains challenging, particularly determining lanes with little- or no-visual-clue, and precise representations of special lanes.

Given good visibility and simple road conditions, traditional vision research methods [1, 2] perform very well. However, they lack robustness in complex real-world scenarios. Recently, various DNN models [3–6] have been trained on large-scale datasets, to infer lane positions via deep semantic features, delivering significantly improved generalization and robustness compared to traditional approaches.

Some research leverages semantic segmentation [3, 5] to identify lanes by classifying pixels or picking up keypoints. However, it is difficult to separate different instances from the lane foreground produced by semantic segmentation for lanes that are very close to each other. Instead, other research turns to a top-down approach. LaneATT [7] first predicts numerous candidates, then post-processes them with non-maximum suppression (NMS). However, NMS struggles to accurately distinguish adjacent lanes, leading to false deletions. CondLaneNet [6] and CANet [8] obtain lane instances by detecting keypoint responses on heatmaps, but due to the local perception characteristics of CNNs, keypoints often respond weakly when visual features are far away from them, making them prone to detection failure. HoughLaneNet [9] leverages DHT-based feature aggregation to detect lanes with weak visual features but is only applicable to straight lanes. To mitigate these challenges, recent studies employing transformer-based models [10–14] utilize a global attention mechanism to derive implicit semantic insights. O2SFormer [13] proposed one-to-several label assignment to address label semantic conflict. Chen [14] improved the convolutional kernel generation network of CondLaneNet with transformer: the object query, after being processed by attention calculation, results in generated kernels possessing more global information. However, these methods do not thoroughly utilize target lo-

TSINGHUA
UNIVERSITY PRESS
Springer



Fig. 1 Lane prediction results using the current state-of-the-art method (CLRNet) and LDTR for cases with little- or no-visual-clue, lens flare, weak lighting, occlusion, and hidden lines. CLRNet misses certain lanes, while LDTR correctly finds all instances. Examples with ground truth are from the CULane dataset.

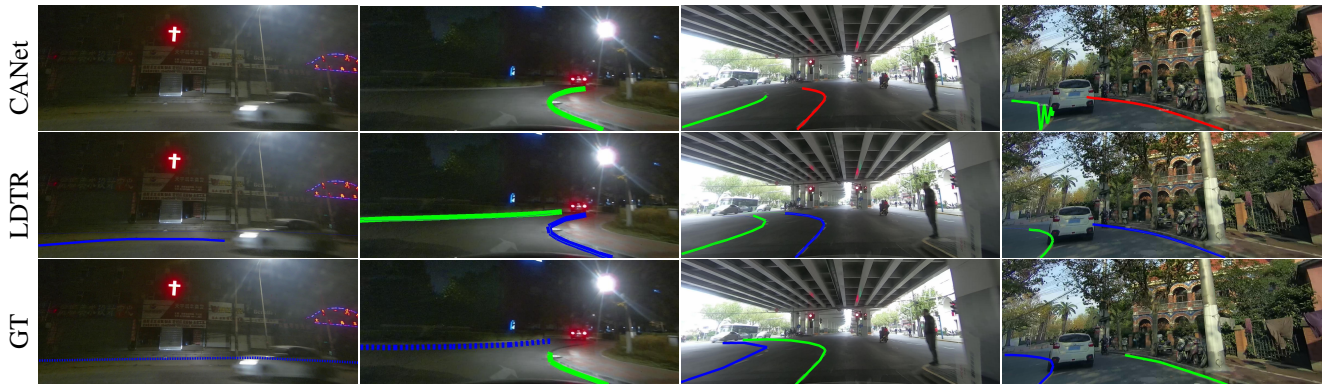


Fig. 2 Lane prediction results for CANet and LDTR for examples from the CurveLanes dataset. Limited by its lane representation, CANet cannot describe lanes in special cases like T-junctions, roundabouts, waiting areas, and sharp turns, while LDTR can address them all.

cations to focus attention. Therefore, a substantial amount of the attention computation is squandered on the background, which is irrelevant to the target objects, thereby restricting the models' ability to effectively discern and focus on the lanes. Fig. 1 illustrates challenging cases, particularly those with few or no visual cues. These cases are crucial for common downstream tasks, such as lane keeping and map-based lane information collection.

Additionally, current lane representations are unsuitable for cases like those in Fig. 2. Existing methods usually rely on handcrafted post-processing rules based on prior assumptions. Almost all methods [5, 6, 13–17] assume that lanes extend from the bottom of the image upwards, so fail to detect horizontal lanes like those in the first three columns of Fig. 2. Although CANet used an adaptive post-processing decoder to avoid such assumptions, it still cannot handle cases like the one in the last column of Fig. 2 due to its reliance on manual settings. It is crucial to develop improved representations that can accurately capture such lanes, as they are commonly encountered in everyday driving.

To tackle the aforementioned problems, we propose a novel

top-down end-to-end lane detection network, termed LDTR (*lane detection transformer*), based on the transformer architecture. Specifically, we propose a novel *anchor-chain* to represent the shapes of lanes and two new loss functions to supervise their overall trend and detailed descriptions. Moreover, to enhance LDTR's ability and efficiency during deep semantic information extraction, a novel *multi-referenced deformable cross-attention* (MRDA) algorithm is applied in the transformer decoder. Additionally, we incorporate auxiliary branches to extract more fine-grained target information. As the second row of Fig. 2 shows, LDTR demonstrates remarkable performance in handling diverse challenging scenarios. Extensive experimental results on multiple datasets [3, 18] show that LDTR achieves state-of-the-art performance.

The main contributions of this paper are as follows:

- A new lane representation method *anchor-chain* is proposed. It conceptualizes lanes as a holistic entity of interconnected nodes, in contrast to the conventional approach of representing them as isolated dots (pixels or keypoints). This allows us to bypass the need for rule-based post-processing and the complexities associated

with handling intricate lane geometries. Moreover, the anchor-chain requires only a few points to denote the important turning points of a lane, so is efficient and precise.

- A *multi-referenced deformable attention module* is proposed to transmit the position prior information contained in the anchor-chain to the network, evenly distributing attention around the targets. This, combined with the global semantic information extracted by the Encoder, enhances the model’s perception ability toward the targets in case of little- or no-visual-clue.
- Two line IoU algorithms are devised, namely the *point-to-point* (P2P) IoU and the *dense-sampling* (DS) IoU. They are applied in binary matching cost and loss during training, respectively. Compared to the traditional point-to-point L1 distance, the new algorithms introduce global optimization to improve training efficiency and inferencing performance.
- We evaluate LDTR using typical metrics, parameterized F1-score as well as synthetic metrics, on public datasets. Experimental results demonstrate that LDTR outperforms other methods overall.

2 Related Work

We relate our work to both the existing lane detection approaches as well as to general object detection methods.

2.1 Lane Detection

Deep learning-based lane detection algorithms can be boiled down into two main categories: *bottom-up* and *top-down*.

Bottom-up methods cluster or classify lane pixels or keypoints. Pixel-level segmentation [3–5], evolving from general visual semantic segmentation, first extracts foreground lane pixels using semantic segmentation and then clusters or classifies them using techniques like pixel embedding to differentiate lane instances. In contrast, keypoint-based detection methods [15, 16] can be regarded as sparse versions of segmentation models that replace dense pixel classification with discrete keypoints, which partially alleviates the problem of excessive focus on segmentation boundaries in pixel-level segmentation. However, bottom-up methods are usually unable to handle branching or merging lanes, and to accurately distinguish adjacent boundaries of multiple closely located lanes. LDTR is designed to address all such challenges.

Top-down methods first obtain target instances and then refine the representation of the shape for each instance. Basically, there are three major categories based on the lane representation: parameterized curve fitting [10, 19], a tilted anchor [7, 13, 20, 21], and row-wise classification [6, 9, 14, 17].

Curve fitting models complex lanes as simple polynomial curves, which can be very efficient due to the small number of descriptors that need to be predicted. However, it is difficult for such curves to match sophisticated lanes in the real world, leading to poor precision and flexibility. Tilted anchor based methods obtain a large number of proposals by placing dense anchors, then filter out unqualified and overlapping instances through NMS in a post-processing stage. However, double solid lines and adjacent lanes are placed close together under specific perspectives and may be incorrectly deleted by NMS during deduplication, leading to critical information loss. In contrast, row-wise classification improves efficiency based on the observation that often, lanes appear vertically. Unfortunately, this also prevents its application to lanes that appear almost horizontally, like high-angle lanes [8] and U-turn lanes.

Unlike these three approaches, LDTR uses set prediction to distinguish lanes that are close together; its anchor ensures precise details while performing well in various complicated cases, such as U-turns, T-junctions, and roundabouts, commonly found in real-world situations and that must be addressed.

2.2 Object Detection

Object detection is closely related to lane detection, and many of its ideas and techniques can be leveraged directly. Early CNN-based methods [22–26] mostly required rule-based post-processing operations, which can lead to poor performance in some uncommon scenarios. DETR [27] proposed a new end-to-end paradigm for object detection but suffers from long training iterations and high computational cost. DETR inspired much following research. Deformable DETR [28] transformed the dense attention operation in the original cross-attention mechanism into a more efficient sparse attention mechanism by reference point sampling, reducing computational cost while improving model training convergence speed. DAB-DETR [29] explicitly modeled the object query as an anchor, using the position of the bounding box to guide attention focus near the target, which further optimizes training and improves model performance.

The global attention mechanism in the DETR paradigm equips the model with a powerful semantic awareness capability, which helps to improve model performance in cases with few or no visual clues. Based on the structures and optimization techniques of the DETR-family, this paper presents an end-to-end lane detection model, LDTR.

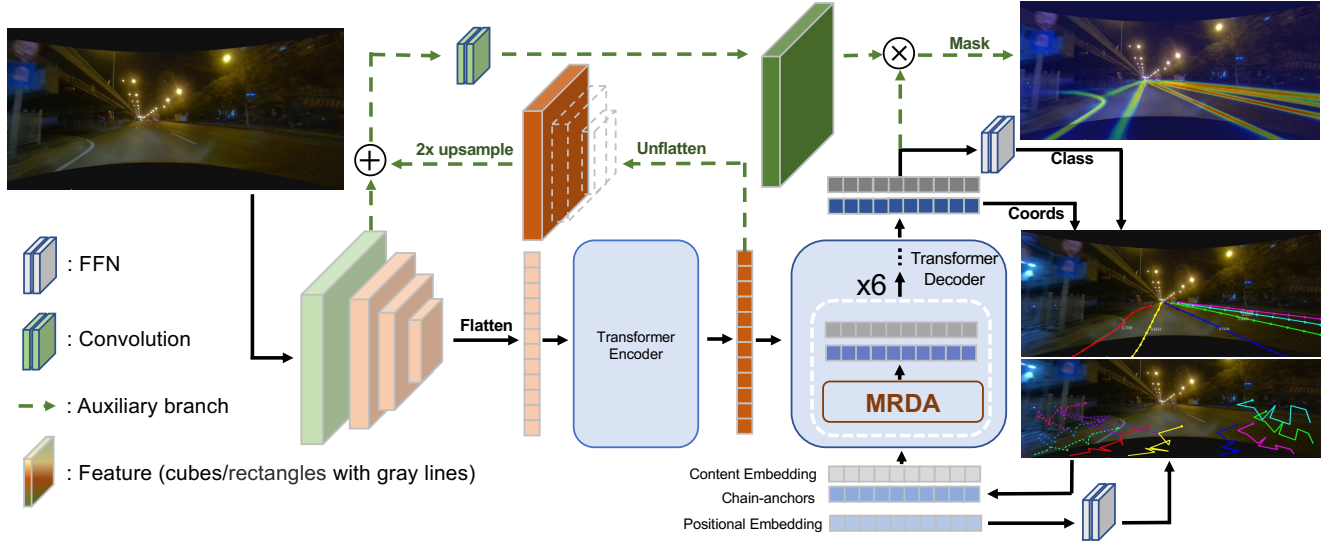


Fig. 3 LDTR follows the structural paradigm of DETR. After 2D image features are extracted by the backbone, LDTR further extracts deep semantic information in the encoder through the self-attention mechanism. The input object queries to the decoder are composed of content embeddings and anchor-chains. In the computation of each decoder layer, the object queries update themselves through MRDA and interact with image features, including the correction of anchor-chains and differentiation of positive or negative objects. After 6 iterative updates, the positive anchor-chains are able to represent lane shapes accurately. Additionally, LDTR introduces a Gaussian heatmap auxiliary branch to enhance the ability of the object query to perceive lane details.

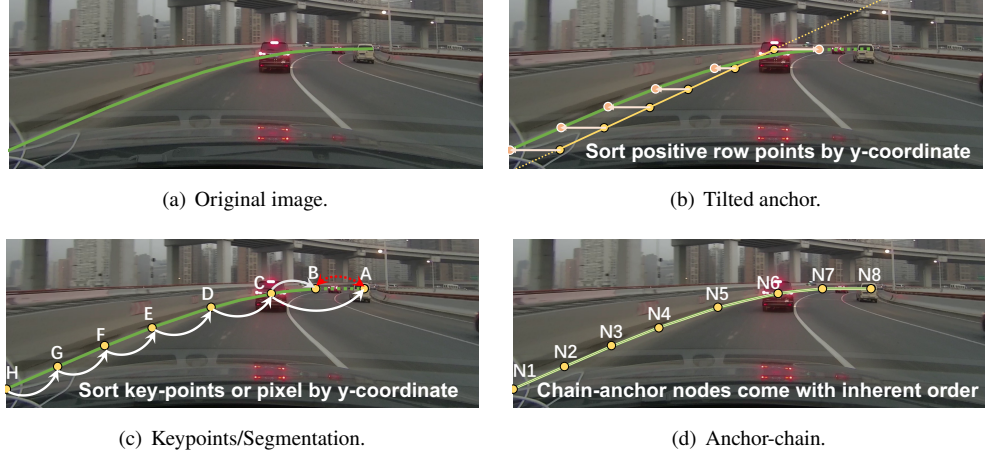


Fig. 4 Various lane representations. It is hard for current methods to represent horizontal parts of lanes, but easy for our anchor-chain.

3 Method

3.1 Network Architecture

As a transformer-based model, LDTR is inspired by the DETR architecture as shown in Fig. 3. The black solid line indicates the lane prediction process. Firstly, LDTR takes a front view as the network input and extracts features at different levels through a backbone network composed of multiple CNN layers. The high-level features are reduced to one dimension and input into the transformer encoder for further interaction and output. Secondly, the transformer decoder takes a small fixed number of learnable content embeddings and anchor-

chains (see Section 3.2) as input object queries, computes MRDA (see Section 3.3) with the output of the encoder, and outputs modified content embeddings and anchors. Finally, the modified content embeddings are passed to a shared parameter feed-forward network (FFN), which predicts the presence or absence of targets, and the anchor-chain accurately describes target positions.

3.2 Anchor-chain

Various lane representations are available, such as tilted anchor lines (see Fig. 4(b) [7]), row-wise classification [6, 17] predicting a set of points and sorting them

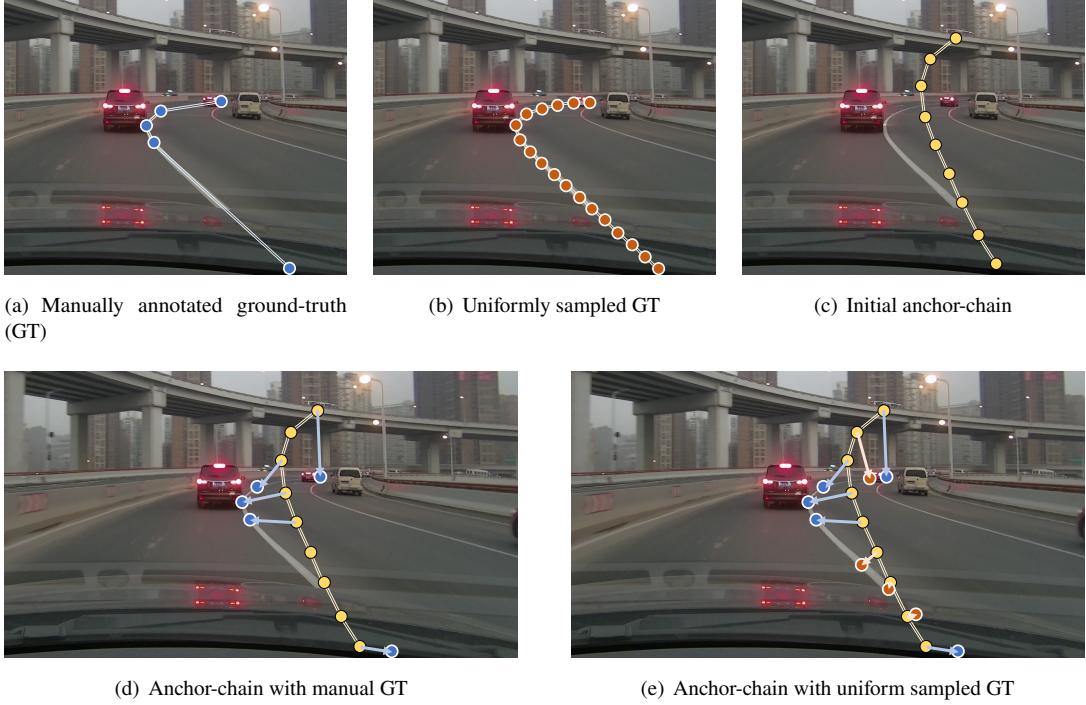


Fig. 5 The regression supervision approach of the anchor-chain enables it to efficiently utilize a small number of nodes to accurately describe curves, essentially similar to how humans recognize lanes.

by y-coordinates [15, 16], and keypoints with adaptive decoders [8] (see Fig. 4(c)). Most share the same assumption that lanes extend vertically in the view. Models with such an assumption usually perform well for such lanes but fail to handle horizontal lanes. Particularly, the tilted anchor does not support curved lanes, while a keypoint-based anchor cannot sort the keypoints properly in case of strongly curving lanes in which y-coordinates are out of order.

To address these challenges, LDTR describes a lane as a whole with a *anchor-chain*, $\text{Lane}_{\text{ca}} = \{(x_1, y_1), \dots, (x_N, y_N)\}$, where N is the number of nodes in the anchor-chain, and x_i, y_i are normalized relative coordinates with values in the range $[0, 1]$ as shown in Fig. 5.

Regarding supervision, LDTR uses two types of ground truth: an ordered set of manually annotated nodes, Lane_m (see Fig. 5(a)), and a densely sampled set of nodes, Lane_s (Fig. 5(b)), obtained by uniform sampling along Lane_m . To predict the lane, Lane_{pr} (see Fig. 5(c), the initial anchor-chain), LDTR first matches it to Lane_m using the Hungarian algorithm [30]. Nodes in Lane_{ca} that have not been successfully matched are then matched with Lane_s using the same algorithm, ensuring that each node in Lane_{pr} is matched to one corresponding ground truth node, forming the final anchor-chain. Finally, LDTR employs L1 distance to supervise the horizontal and vertical coordinates of each predicted

node on the anchor-chain; the loss is:

$$L_{\text{reg}} = -\frac{1}{N} \sum_{(x, y) \in \text{Lane}} |\hat{P}_{xy} - P_{xy}| \quad (1)$$

where \hat{P}_{xy} and P_{xy} denote predicted and ground truth nodes, respectively.

Unlike the uniform sampling in the Point Set approach [31], LDTR samples $M (M \gg N)$ nodes on the annotated lane and performs Hungarian matching between these nodes and predictions. It matches each predicted node to the closest ground truth node, giving the nodes more degrees of freedom. This allows the anchor-chain to learn implicit human preferences in the annotations during training and to distribute the nodes at higher information density at turning points. Besides, thanks to the low prior assumption setting, the anchor-chain can describe lanes of any shape and requires no longer prior conditions.

In addition, the anchor-chain can also provide fine-grained position information for the network. The cross-attention module needs to gather features from the entire feature map, so it is necessary to provide appropriate position priors for each query to focus attention on the locality surrounding the targets. LDTR explicitly models the query position as an anchor, which is a similar approach to DAB-DETR. The anchor-chain can effectively help the network aggregate features from nearby regions of different parts of a target using multi-

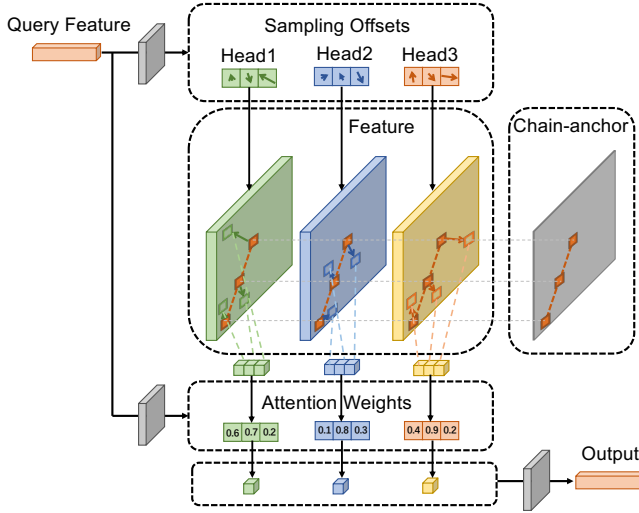


Fig. 6 The multi-referenced deformable cross-attention module leverages positional information from the anchor-chain to guide the attention distribution.

referenced deformable cross-attention modules.

3.3 Multi-Referenced Deformable Cross-Attention

As most adjacent features contain similar appearance information, traditional cross-attention modules bring a lot of additional computation, most of which is useless computation on backgrounds. The improved deformable attention module [32] samples partial information based on a learnable offset field. However, due to the lack of explicit supervision to guide sampling along the object contour, the deformable attention module can still lead to wasted computation when sampling around the center of elongated lanes, and cannot balance sampling of endpoints far away from the center point. Therefore, LDTR uses points (anchors) distributed along the lanes as reference points and samples only part of the information around each point, as shown in Fig. 6. By assigning only a small number of keys along the lanes for each query, the convergence speed and computational efficiency can be improved significantly.

3.4 Line IoU

3.4.1 Background

L1 distance loss (see Equation (1)) can independently optimize the position of each node on the chain, but lacking an overall error calculation of the target nodes leads to slow convergence. IoU loss is a widely adopted overall loss function in object detection/segmentation, computed by bounding box overlap or pixel-level intersection. For thin and long objects such as lanes, the bounding box method suffers from large errors while the latter does not support gradient backpropagation using the current lane representation.

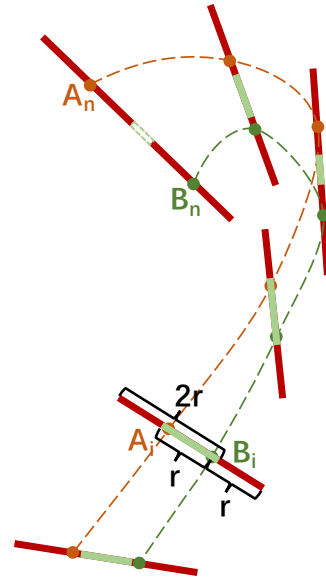


Fig. 7 Point-to-point (P2P) line IoU.

Hence, CLRNet [20] suggested *line IoU*, an approximate IoU algorithm for lanes. However, it assumes lanes are all vertical and only calculates the horizontal errors between two lines. Thus line IoU results for a pair of lines vary a lot when they appear at different angles. In addition, the existing line IoU algorithm is bound to a row-wise classification head and can only describe lanes that extend vertically in the view, which cannot be used to optimize our anchor-chain that can describe lane lines of any shape. To address such limitations, we propose two line IoU algorithms inspired by the Anchor-chain: *point-to-point* and *dense-sampling* Line IoU.

3.4.2 Point-to-Point Line IoU

To calculate the IoU of two lines A and B , the Point-to-Point (P2P) algorithm picks the same number (N) of keypoints on them uniformly and pairs the i -th points together (A_i, B_i). Given a fixed length r , draw two line segments along the direction of (A_i, B_i) with length $2r$, taking A_i and B_i as midpoints, respectively (thick solid red lines in Fig. 7). Let $L_{\cup}^{A_i B_i}$ be the distance between the far endpoints (the union) of the two segments, $L_{\cap}^{A_i B_i}$ the distance between the near endpoints (the intersection, green lines in Fig. 7) and $\|A_i B_i\|_2$ the length of (A_i, B_i) . If the two segments overlap, $L_{\cap}^{A_i B_i} = 2r - \|A_i B_i\|_2$ (solid green lines), while they are separated from each other (like (A_n, B_n) in Fig. 7). This expression is still used instead of 0, describing how far away they are in negative values (thick white line with the dashed green border between A_n and B_n). This is helpful for gradients and

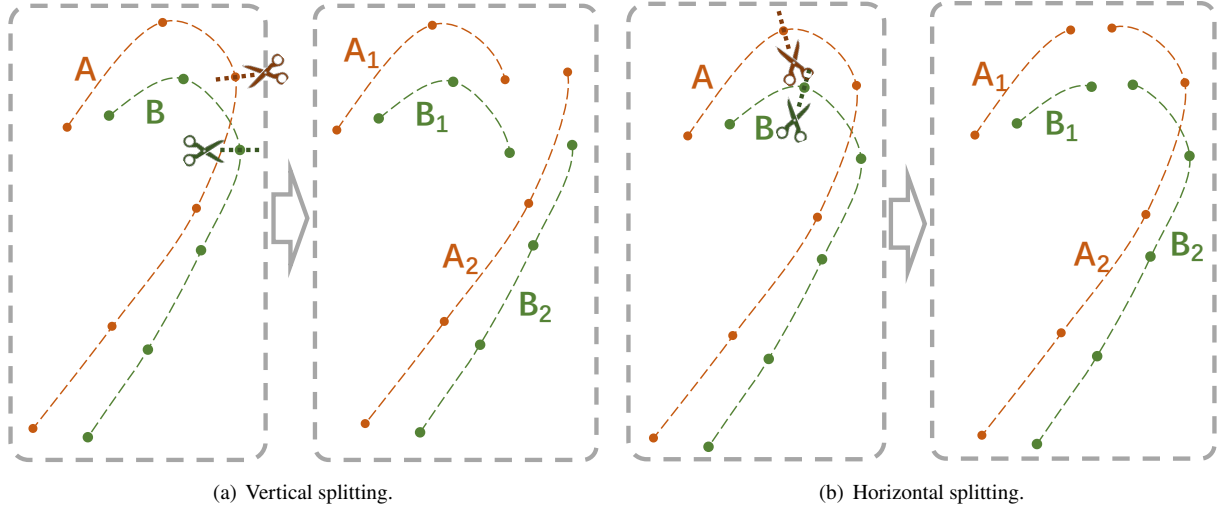


Fig. 8 Split U-turn lines.

optimization. Then, LIoU_{P2P} is defined as Equation (2).

$$\text{LIoU}_{\text{P2P}}(A, B) = \frac{\sum_{i=1}^N L_{\cap}^{A_i B_i}}{\sum_{i=1}^N L_{\cup}^{A_i B_i}} = \frac{\sum_{i=1}^N (2r - \|A_i B_i\|_2)}{\sum_{i=1}^N (2r + \|A_i B_i\|_2)} \quad (2)$$

Fig. 7 illustrates how LIoU_{P2P} is computed. LIoU_{P2P} ranges from -1 to 1. When the two lines overlap completely, it is 1, while when they are infinitely apart, it converges to -1.

P2P line IoU describes the trend similarity between lanes and is not affected by the lane orientation. Thanks to its stability in the optimization process, LDTR leverages P2P line IoU to compute the matching error as a supplement to the L1 distance and classification costs.

3.4.3 Dense-sampling Line IoU

DS line IoU consists of two steps:

Step 1: Line splitting. DS line IoU samples keypoints in both x and y directions. To be compatible with curved lanes and backtracking lanes, it first splits the lines in the sampling direction into multiple one-way line segments. Considering Fig. 8, after the lines A and B are split, they respectively consist of line segments $\{A_1, A_2\}$ and $\{B_1, B_2\}$, each of which contains multiple sample points.

Step 2: Segment-wise calculation. For each unidirectional sub-line, the algorithm sets reference lines for every distance d in the sampling direction. If a reference line intersects both line segments, the two intersection points are paired together as in P2P, in which case DS shares the definitions of L_{\cap} and L_{\cup} with P2P in Equation (3).

$$\begin{aligned} L_{\cap}^{A_{ij} B_{ij}} &= 2r - \|A_{ij} B_{ij}\|_2 \\ L_{\cup_2}^{A_{ij} B_{ij}} &= 2r + \|A_{ij} B_{ij}\|_2 \end{aligned} \quad (3)$$

where i is the segment index, j the reference point index, 2

in \cup_2 refers to the number of intersection points.

Otherwise, if a reference line intersects only one sub-line, L_{\cap} is set to 0, and L_{\cup_1} is set as below.

$$L_{\cup_1}^A = L_{\cup_1}^B = 2r \quad (4)$$

Fig. 9 illustrates how the reference lines intersect the segments and cases of different intersection points.

Then, DS line IoU is defined as the ratio of accumulated intersection distances to the union ones as in P2P:

$$\text{LIoU}_{\text{DS}}(A, B) = \frac{\sum_{i=1}^O \sum_{j=1}^{N_i} L_{\cap}^{A_{ij} B_{ij}}}{\sum_{i=1}^O \sum_{j=1}^{N_i} L_{\cup_2}^{A_{ij} B_{ij}} + \sum_{i=1}^{U_A} L_{\cup_1}^A + \sum_{i=1}^{U_B} L_{\cup_1}^B} \quad (5)$$

where O is the number of \cup_2 segments, N_i the number of sampling points in the i -th \cup_2 segment, and U_A and U_B are the numbers of \cup_1 segments on lines A and B , respectively.

Changing the sampling interval d can make a flexible balance between precision and speed. LDTR sets d to 8 pixels by default. While DS requires more computation than P2P, it is straightforward to parallelize the algorithm on the GPU.

LDTR applies DS line IoU to the overall loss of the target as shown in Equation (6), which can record subtle differences between the predictions and GT. Since the entire chain of nodes is considered as a whole, the predictions of the horizontal and vertical coordinates are optimized in x and y directions independently.

$$L_{\text{iou}} = 1 - \text{LIoU}_{\text{DS}}(P_{\text{chain}}, \hat{P}_{\text{chain}}) \quad (6)$$

where P_{chain} and \hat{P}_{chain} are the ground truth and predicted chains, respectively.

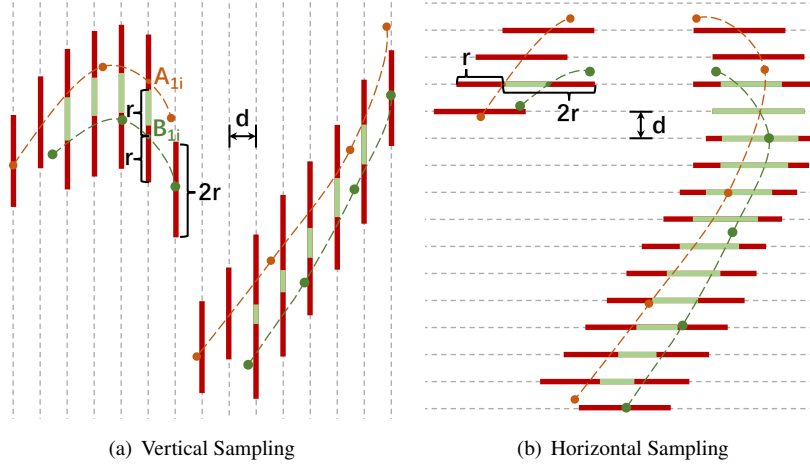


Fig. 9 Dense-Sampling (DS) Line IoU.

3.5 Gaussian Heatmap Auxiliary Branch

Multi-task training has been widely used to enhance the generalization ability of single-task models. Therefore, LDTR introduces a Gaussian heatmap branch [8] as an auxiliary training branch. The structure and workflow of the branch are similar to that of Mask-DINO [33], as indicated by the green dotted line in Fig. 3.

The Gaussian heatmap auxiliary training branch only performs forward and backward propagation during the training process, and the gradient is backpropagated to update the network weights. During inferencing, this branch is discarded for efficiency. Networks with auxiliary branches have more parameters, making it easier to learn how to fit the relationship between input images and ground truth from the initial state, effectively improving the rate of convergence and stability of the optimization direction of the model. LDTR uses the same L_{mask} and L_{offset} as CANet to supervise training of the auxiliary branch.

3.6 Total Loss

In addition, LDTR adopts Focal loss to supervise the classification head following DETR. It is used to determine whether each query corresponds to a target in the input. The classification loss is:

$$L_{\text{cls}} = \frac{-1}{N_Q} \sum_{q \in Q} \begin{cases} (1 - \hat{P}_q)^\gamma \log \hat{P}_q & P_q = 1 \\ (1 - P_q)^\lambda \hat{P}_q^\gamma \log(1 - \hat{P}_q) & \text{otherwise} \end{cases} \quad (7)$$

where Q represents the set of all queries, P_q and \hat{P}_q denote the prediction and binary match ground truth for Query q , respectively, and N_Q is the number of queries. The total loss function in LDTR is then:

$$L_{\text{total}} = aL_{\text{cls}} + bL_{\text{reg}} + cL_{\text{iou}} + L_{\text{mask}} + L_{\text{offset}} \quad (8)$$

The hyperparameters a , b , and c are set to 1, 5, and 1, respectively.

4 Experiments

4.1 Datasets

To evaluate LDTR, extensive experiments were conducted on two widely used datasets for lane detection, CULane [3] and CurveLanes [18]. As a comprehensive dataset, CULane contains images from urban street views, rural roads, and highways under diverse conditions, e.g. with glare and occlusion. Many lanes have little- or no-visual-clue, and lane detection requires a deep understanding of the overall scene by the models as demonstrated in Fig. 1. While lanes in CurveLanes are more obvious than those in CULane, CurveLanes has more topologically complicated lanes, such as forks, convergences, sharp turns, and T-junctions as seen in Fig. 2, which were not well addressed in earlier datasets.

4.2 Performance Metrics

4.2.1 Parameterized F1-score

F1-score is the default evaluation metric for lane detection models. Predictions and ground truth are expanded into fixed-width masks and the IoU between masks greater than the threshold is regarded as TP. The default IoU threshold of 0.5 originated from general object detection but is too high for lane detection. Because lanes are long, thin objects, slight jitter in predicted points may lead to huge IoU variation. IoU is so sensitive that many predictions may be rejected even though they are suitable for downstream tasks. The situation would get worse for cases in Fig. 10.

On the one hand, many lanes lack obvious visual features to provide sufficient information for models to accurately



Fig. 10 Abnormal predictions with typical IoU threshold. Thin solid lines are ground truth, and thick dotted ones are predicted lanes. Dist indicates the Fréchet distance between the prediction and corresponding ground truth.

locate. Some predicted lanes run almost parallel to the ground truth at a tiny distance, like the predictions with IoU of 0.34, 0.35, 0.28, and 0.21 in Fig. 10(a). These predictions should be allowed but are dropped because of the small IoU. Hence, it is reasonable to decrease the threshold of IoU to allow predictions with inaccurate but acceptable locations. Looking at Fig. 10(a), the threshold could be adjusted from 0.5 to 0.2.

On the other hand, certain high IoU predictions should not be accepted because IoU only focuses on pixel overlap but lacks measurement of lane trends, as Fig. 10(b) illustrates. Specifically, two situations cause such misjudgments: incomplete prediction and incorrect trend prediction, both of which are harmful to real-world downstream tasks. Simply decreasing the IoU threshold may exacerbate the occurrence of such misjudgments, so Fréchet distance is introduced to filter out predictions that deviate significantly from the real trend. The original Fréchet distance expects the lines to be roughly the same length and calculates the maximum shortest distance bidirectionally. However, concerning lane detection, the predicted lanes may be longer than the ground truth. Though the additional predicted segment implies the lane

trend, it is difficult to justify and should be weighted less.

Thus, we modify Fréchet distance to calculate unidirectionally from ground truth to predictions only, to make sure every point in ground truth counts but not vice versa. Predicted lanes are then considered to match only if they satisfy a hybrid constraint: $\text{IoU} \geq \alpha$ and $\text{Fréchet distance} \leq \beta$. Thus, the F1-score will depend on two parameters, IoU threshold (α) and Fréchet distance threshold (β): $\text{F1} = \text{F1}(\alpha, \beta)$. The classic F1-score configuration corresponds to $\text{F1}(0.5, +\infty)$, while in our experiments we set β to be 4% of the image width, i.e., $\text{F1}(0.2, 60)$ for CULane and $\text{F1}(0.2, 10)$ for CurveLanes. For simplicity, F1 without qualification means $\text{F1}(0.5, +\infty)$ in the following unless otherwise specified. Not only lane detection, but also other object detection tasks could benefit from the idea of parameterized F1-score.

The video in the supplementary material compares the prediction results of the current state-of-the-art model CLRNet and LDTR on CULane using two different evaluation metrics. The video visually demonstrates that LDTR has better instance recall in situations where visual cues are lacking. However, these additional recalls compared to CLRNet are

Table 1 Performance of state-of-the-art models and LDTR on CULane. Prec = Precision; PF1 = F1(0.2, 60).

Model	F1	Prec	Recall	MIoU	MDis	PF1
CANet	79.86	88.03	73.08	82.61	15.83	81.85
CLRNet	80.47	87.13	74.77	82.13	22.62	82.11
LDTR	78.16	81.53	75.06	82.23	12.89	84.18

Table 2 LDTR performance by adopting the two IoU algorithms in different cost and loss combinations. Prec = Precision; PF1 = F1(0.2, 10).

Cost	Loss	F1	Prec	Recall	MIoU	MDis	PF1
N/A	N/A	86.24	88.20	84.36	79.86	2.88	88.60
P2P	P2P	87.15	90.92	83.69	81.25	2.77	88.51
DS	DS	87.74	90.28	85.33	81.19	2.86	89.00
P2P	DS	87.96	91.19	84.95	81.31	2.85	89.01

often regarded as false positives (red lines).

4.2.2 MIoU and MDis

In Fig. 10, all predictions of IoU below 0.5 are dropped by F1 because they are regarded as false positives, though they are suitable for downstream tasks and should be accepted instead. Consequently, if a model predicts more lanes of this kind, its precision will become worse. This contradiction stems from the definition of precision, and more insightful indicators are required to investigate lane detection models together.

Thus, we suggest turning to *MIoU* (Mean IoU) and *MDis* (Mean Fréchet Distance), defined as

$$\text{MIoU} = \frac{\sum_{i \in U_{\text{TP}}} \text{IoU}_i}{N_{\text{TP}}}, \quad \text{MDis} = \frac{\sum_{i \in U_{\text{TP}}} \text{Dis}_i}{N_{\text{TP}}}, \quad (9)$$

to compare position precision and trend similarity of predicted lanes under similar recall rates. Both metrics describe how closely the predictions relate to ground truth overall, which makes more sense than precision with respect to lane detection. Here, N_{TP} is the number of true positive predictions, and U_{TP} is the set of all true positive instances.

4.2.3 Necessity of New Metrics

To verify the effectiveness of the synthetic metrics, experimental results for current leading models and LDTR are presented in Table 1. Some valuable insights can be gained from the results. Although CLRNet reaches the best F1 and precision, LDTR has a better recall rate. Additionally, with superior MIoU and MDis, LDTR predicts lane positions more accurately. CANet has the highest precision and MIoU due to its adaptive decoder's great description ability for common lanes, and a little degradation in recall rate. Overall, the highest F1(0.2, 60) of LDTR indicates that some false positive predictions otherwise are correctly recalled, while the smallest MDis guarantees these predictions are safe.

4.3 Evaluation of Line IoU Algorithms

Line IoU can be used as a binary matching cost to improve the stability of matching, or as a loss function to optimize model training. Table 2 presents LDTR performance using the two proposed IoU algorithms in different combinations. Both algorithms adopted as either cost or loss function outperform the baseline, while P2P is more suitable for cost and DS for loss. This is because P2P is insensitive to shape jitter, so using P2P as the cost for bipartite matching can make the training more stable, while DS can capture subtle differences and is intrinsically suitable for the loss function, to optimize prediction details.

4.4 Ablation Study

Table 3 presents the results of an ablation study of the different components of LDTR, using the CurveLanes dataset. Unlike other lane description methods that directly perform local computation on the image feature map, the transformer encoder-decoder query-based structure adopted in this paper does not have a strong mapping relationship between the query representing each lane instance and positions in the image. If replacing anchor-chain with other methods, the entire decoder needs to be removed, making it impossible to control variables effectively. Therefore, we have to keep anchor-chain in the baseline. The baseline (1st row) is the DETR-based model with anchor-chain, which utilizes the classification loss (L_{cls} as Equation (8)) and regression loss (L_{reg} as Equation (1)).

In the 2nd row, the original deformable attention is replaced with MRDA, whose attention positions are shown in Fig. 11. Because of the more precise location prior, MRDA can focus on more comprehensive detailed features, which boosts all metrics in the results.

Particularly, when line IoU is adopted (3rd row) in the loss and matching error, the calculation optimizes each lane instance as a whole, thus significantly improving the accuracy and MIoU. In the last row, F1(0.2, 60) and MDis are improved remarkably, indicating the auxiliary branch can enhance the model to extract global semantic information.

4.5 Performance on Datasets

4.5.1 Results on CULane

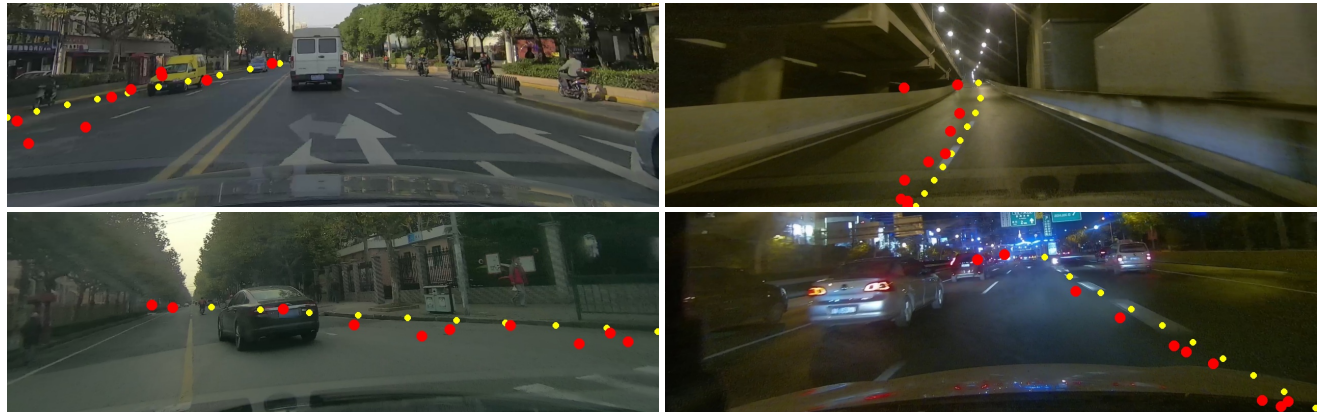
As mentioned in Section 4.1, in CULane, many lanes have little- or no-visual-clue, so it is suitable to distinguish the recall capabilities of different models. Table 4 presents our comprehensive experimental results. Models are clustered according to their basic techniques into CNN-based and

Table 3 Ablation experiments of different components in LDTR on CurveLanes.

No.	Model	F1	Precision	Recall	MIoU	MDis	F1(0.2, 10)
1	Anchor-chain	85.57	87.41	83.80	78.86	3.01	88.44
2	+MRDA	86.24 _{+0.67}	88.20 _{+0.79}	84.36 _{+0.56}	79.86 _{+1.00}	2.88 _{-0.13}	88.60 _{+0.16}
3	+Line-IoU	87.96 _{+1.72}	91.19 _{+2.99}	84.95 _{+0.59}	81.31 _{+1.45}	2.85 _{-0.03}	89.01 _{+0.41}
4	+Auxiliary	88.44 _{+0.48}	91.55 _{+0.36}	85.53 _{+0.58}	81.39 _{+0.08}	2.69 _{-0.16}	89.66 _{+0.65}



(a) Original deformable attention (ODA).



(b) Multi-referenced deformable attention (MRDA).

Fig. 11 Distribution of reference points (yellow) and sample points (red) in cross-attention modules. In MRDA, the attention tends to be distributed along the line, while in ODA, the attention is often concentrated near the central point.

transformer-based groups, and best results are marked in bold in each group. LDTR is ahead of other Transformer-based models in almost all categories, validating the effectiveness of LDTR’s network structure design. However, it lags behind CLRNet because CNN-based models often predict fewer false positives, which results in higher precision and F1. As discussed in Section 4.2, F1 and precision are not the most appropriate metrics for downstream tasks using lane detection, so an additional test measured F1(0.2, 60) for various leading methods. LDTR outperforms both CANet and CLRNet by 2.33 and 2.07 overall, respectively, especially for scene types with fewer visual clues such as Crowded, Dazzle, and Shadow. It is worth noting that LDTR’s F1(0.2, 60) score is significantly

improved (by 6.02 percentage points) compared to its overall F1 score. This is because, for the no-visual-clue scenarios that exist in CULane, LDTR’s predictions are recalled more frequently using a more reasonable true positive standard. CLRNet and CANet have weaker recall performance in this scenario, resulting in poorer performance than LDTR as assessed by F1(0.2, 60).

4.5.2 Results on CurveLanes

Compared to CULane, the CurveLanes dataset covers a wider range of scenes and has more complicated lane shapes, so provides a better test of lane shape modeling ability. Table 5 shows the test results in detail. LDTR performs best in terms of both F1 and F1(0.2, 10), especially for recall rate, which is

Table 4 Comparative testing on CULane. The first two groups (CNN-based and Transformer-based) are measured using the F1 metric, while selected state-of-the-art, SOTA, methods are assessed using F1(0.2, 60) in the final group.

	Method	Total	Normal	Crowded	Dazzle	Shadow	No line	Arrow	Curve	Cross	Night
CNN-based (F1)	SCNN	71.60	90.60	69.70	58.50	66.90	43.40	84.10	64.40	1990	66.10
	CurveLane	74.80	90.70	72.30	67.70	70.10	49.40	85.80	68.40	1746	68.90
	LaneATT	77.02	91.74	76.16	69.47	76.31	50.46	86.29	64.05	1264	70.81
	CondLaneNet	79.48	93.47	77.44	70.93	80.91	54.13	90.16	75.21	1201	74.80
	GANet	79.63	93.67	78.66	71.82	78.32	53.38	89.86	77.37	1352	73.85
	CANet	79.86	93.60	78.74	70.07	79.35	52.88	90.18	76.69	1196	74.91
Transformer-based (F1)	CLRNet	80.47	93.73	79.59	75.30	82.51	54.58	90.62	74.13	1155	75.37
	PriorLane	76.27	92.36	73.86	68.26	78.13	49.60	88.59	73.94	2688	70.26
	LaneFormer	77.06	91.77	75.41	70.17	75.75	48.73	87.65	66.33	19	71.04
	LDTR	78.16	93.22	75.91	72.57	79.53	53.02	88.70	70.41	1352	73.66
SOTA (F1(0.2, 60))	CANet	81.85	95.45	80.57	77.43	77.99	55.45	91.68	71.22	1196	77.10
	CLRNet	82.11	94.54	80.85	80.96	81.14	58.66	91.85	58.33	1155	78.80
	LDTR	84.18	96.12	83.27	81.49	87.39	62.93	92.06	62.77	1352	81.52

Table 5 Performance comparison on CurveLanes. The first group models are measured in F1, while the second group is in F1(0.2, 10) (marked with “*”).

Models	F1	Precision	Recall	FPS
SCNN	65.02	76.13	56.74	7.5
ENet-SAD	50.31	63.60	41.60	75
PointLaneNet	78.47	86.33	72.91	71
CurveLane	82.29	91.11	75.03	-
CondLaneNet	86.10	88.98	83.41	48
CANet	87.87	91.69	84.36	36.6
LDTR	88.44	91.55	85.53	25.2
CANet*	88.48	92.33	84.95	36.6
LDTR *	89.66	92.82	86.72	25.2

Table 6 Average performance comparison on CULane and CurveLanes. As CLRNet did not provide metrics and trained weights on CurveLanes, it is not included.

Datasets	Models	AF1	AP	AR
CULane	CANet	62.97	69.85	57.33
	CLRNet	58.99	63.87	54.81
	LDTR	63.65	66.39	61.12
CurveLanes	CANet	58.55	61.10	56.22
	LDTR	62.76	65.06	60.62

emphasized by LDTR.

4.5.3 Average Performance

All previous experiments were executed with fixed hyperparameters α and β . To evaluate the capability of LDTR with different hyperparameter configurations, we borrowed the COCO [34] object detection dataset performance indicators AP and AR and define AF1 (average F1-score) similarly. By conducting extensive experiments with many α, β combinations, Table 6 shows that LDTR surpasses other networks on average, implying the effectiveness of its architectural design, independent of specific parameter settings.

To thoroughly understand how the Fréchet distance threshold is determined, Figs. 12 and 13 present how F1-score varies with Fréchet distance thresholds with different IoU

settings for the two datasets, respectively. LDTR generally performs better than the other two models, especially, when the IoU threshold is small. As the IoU threshold increases, no-visual-clue lanes are more likely to be dropped, thus the advantage of LDTR gradually diminishes. These figures indicate that LDTR exceeds in F1-score over a wide range of Fréchet distance thresholds.

5 Visual Comparison

For a more intuitive comparison, we have selected and included several frames in Fig. 14. These scenes include different lighting conditions, occlusions and most have no-visual-clue for lanes. Considering the ground truth shows that LDTR can determine nearly all the instances while CLRNet misses some. However, those predictions recalled by LDTR but missed by CLRNet are often mistakenly identified as false positives in the default evaluation metric (F1(0.5, $+\infty$)), leading to an underestimation of model performance. The use of the F1(0.2, 60) evaluation metric can partially alleviate such misjudgment and provide a more objective and comprehensive evaluation of model performance.

6 Conclusions and Future work

There are still fundamental challenges in lane detection to be addressed: predicting lanes with little- or no-visual-clue, and describing lanes of any shape. Aiming at these goals, this paper proposes LDTR, a transformer-based network, to leverage the global perceptual ability of transformers to improve the instance recall capability. The anchor-chain representation enables LDTR to model lanes flexibly and precisely. To speed up convergence and reduce computation, a multi-referenced deformable cross-attention module is proposed to work together with the anchor-chain. In addition, two line IoU algorithms are presented to underpin the cost and loss functions, which

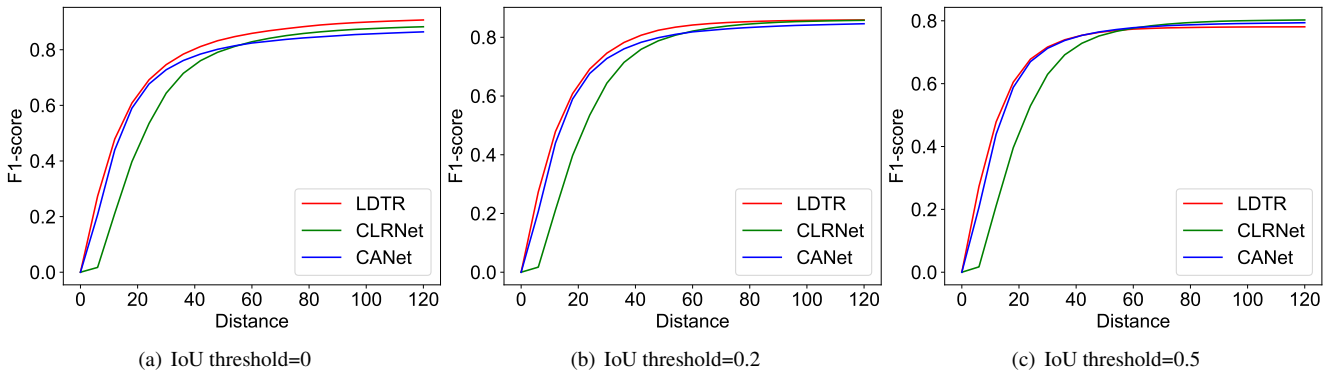


Fig. 12 F1-scores of different models vs. Fréchet distance thresholds on CULane.

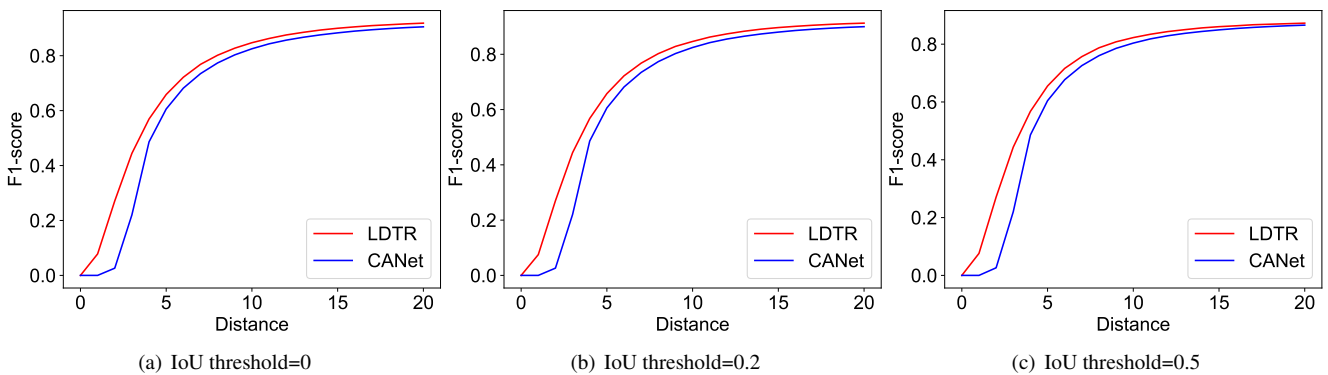


Fig. 13 F1-scores of different models vs. Fréchet distance thresholds on CurveLanes. As CLRNet did not provide metrics and trained weights on CurveLanes, it is not included.

further enhances LDTR's representation capability along with the auxiliary branch. Considering the differences between lanes and typical objects, the F1-score is extended to accept Fréchet distance as an additional parameter besides reducing the IoU threshold. Meanwhile, several synthetic metrics are devised to evaluate LDTR along with classic metrics. Our experimental results show that LDTR achieves state-of-the-art performance on two well-known datasets.

In the future, we plan to first improve the inference speed of LDTR (it is currently the slowest approach in Table 5). In addition, the temporal information implied in the video can provide valuable insights when there are no-visual-clue for lanes in the following frames. Existing methods, such as RVLD [21], take advantage of this. In real-time videos, we will investigate sharing semantic information between frames by utilizing updated queries in the decoder.

Electronic Supplementary Material

A demo video is available in the online version of this article, which shows how LDTR and CLRNet (the current SOTA model) perform on CULane validation set.

The frame is divided into four parts. The upper and lower

background areas of the frame represent the prediction results of LDTR and CLRNet respectively, where green and red lines indicate TP (true positive) and FP (false positive) respectively measured in the default evaluation metric. The picture-in-picture area in the upper part of the frame also displays the prediction results of LDTR, but using the F1(0.2, 60) evaluation metric. The picture-in-picture area in the lower part of the frame shows the GT (ground truth).

Declarations

Availability of data and materials

The datasets analyzed during the current study are available in the following repositories: <https://github.com/SoulmateB/CurveLanes> and <https://xingangpan.github.io/projects/CULane.html>.

Competing interests

The authors have no competing interests to declare that are relevant to the content of this article.

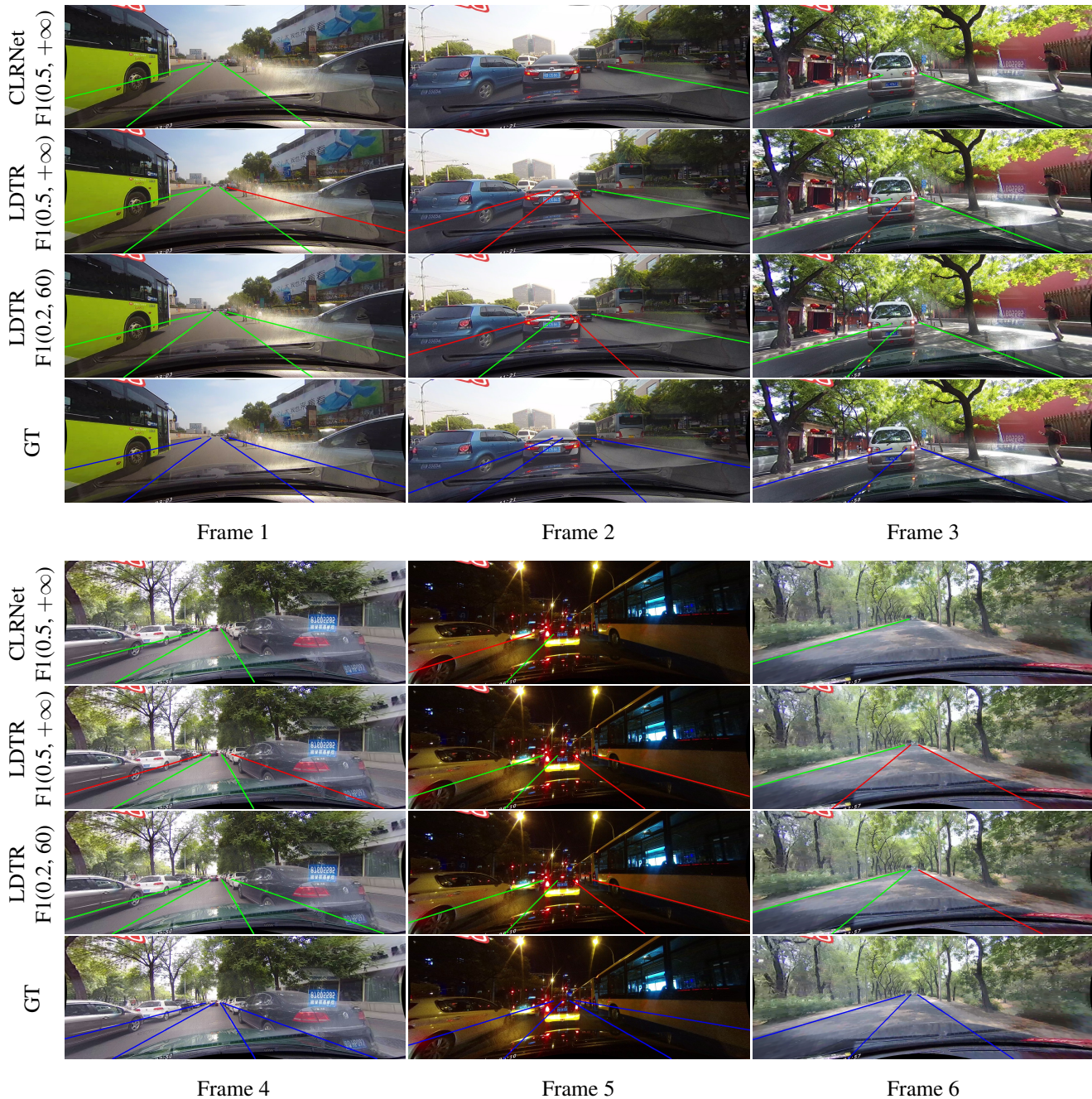


Fig. 14 Prediction ability comparison between CLRNet and LDTR for “Congested Scenarios” in CULane. The green and red lines represent the true positive (TP) and false positive (FP) of the model’s prediction results under a specific evaluation indicator, respectively, while the ground truth (GT) is represented by blue lines.

Funding

This paper was supported by the National Natural Science Foundation of China (No. U23A6007).

Author contributions

Zhongyu Yang, Chen Shen and Wei Shao conceived of the presented idea, Zhongyu Yang proposed and implemented

the prototype system. Zhongyu Yang, Chen Shen, Wei Shao and Tengfei Xing designed and performed the experiments and analyzed the data. Runbo Hu, Pengfei Xu, Hua Chai and Ruini Xue supervised the project. Ruini Xue contributed to the interpretation of the results and took the lead in writing the manuscript. All authors discussed the results and contributed to the final manuscript.

Acknowledgements

We would like to express our sincere gratitude to Xingxu Yao and Yueming Zhang for their valuable assistance in analyzing the experimental results. We would also like to thank Ge Zhang for her valuable insights and assistance in refining the wording of the paper.

References

- [1] Kim Z. Robust lane detection and tracking in challenging scenarios. *IEEE Transactions on intelligent transportation systems*, 2008, 9(1): 16–26.
- [2] Borkar A, Hayes M, Smith MT. Robust lane detection and tracking with ransac and kalman filter. In *2009 16th IEEE International Conference on Image Processing (ICIP)*, 2009, 3261–3264, doi:10.1109/ICIP.2009.5413980.
- [3] Pan X, Shi J, Luo P, Wang X, Tang X. Spatial as deep: Spatial cnn for traffic scene understanding. In *Proceedings of the AAAI Conference on Artificial Intelligence*, 1, 2018, 7276–7283.
- [4] Neven D, De Brabandere B, Georgoulis S, Proesmans M, Van Gool L. Towards end-to-end lane detection: an instance segmentation approach. In *2018 IEEE intelligent vehicles symposium (IV)*, 2018, 286–291, doi:10.1109/ivs.2018.8500547.
- [5] Abualsaud H, Liu S, Lu DB, Situ K, Rangesh A, Trivedi MM. Laneaf: Robust multi-lane detection with affinity fields. *IEEE Robotics and Automation Letters*, 2021, 6(4): 7477–7484.
- [6] Liu L, Chen X, Zhu S, Tan P. Condlanenet: a top-to-down lane detection framework based on conditional convolution. In *Proceedings of the IEEE/CVF International Conference on Computer Vision*, 2021, 3773–3782.
- [7] Tabelini L, Berriel R, Paixao TM, Badue C, De Souza AF, Oliveira-Santos T. Keep your eyes on the lane: Real-time attention-guided lane detection. In *Proceedings of the IEEE/CVF conference on computer vision and pattern recognition*, 2021, 294–302.
- [8] Yang Z, Shen C, Shao W, Xing T, Hu R, Xu P, Chai H, Xue R. CANet: Curved Guide Line Network with Adaptive Decoder for Lane Detection, 2023.
- [9] Zhang JQ, Duan HB, Chen JL, Shamir A, Wang M. Hough-LaneNet: Lane detection with deep hough transform and dynamic convolution. *Computers & Graphics*, 2023, 116: 82–92.
- [10] Liu R, Yuan Z, Liu T, Xiong Z. End-to-end lane shape prediction with transformers. In *Proceedings of the IEEE/CVF winter conference on applications of computer vision*, 2021, 3694–3702.
- [11] Qiu Q, Gao H, Hua W, Huang G, He X. PriorLane: A Prior Knowledge Enhanced Lane Detection Approach Based on Transformer. *arXiv preprint arXiv:2209.06994*, 2022.
- [12] Han J, Deng X, Cai X, Yang Z, Xu H, Xu C, Liang X. Laneformer: Object-aware Row-Column Transformers for Lane Detection. In *Proceedings of the AAAI Conference on Artificial Intelligence*, 1, 2022, 799–807.
- [13] Zhou K, Zhou R. End to End Lane detection with One-to-Several Transformer. *arXiv preprint arXiv:2305.00675*, 2023.
- [14] Chen Z, Liu Y, Gong M, Du B, Qian G, Smith-Miles K. Generating Dynamic Kernels via Transformers for Lane Detection. In *Proceedings of the IEEE/CVF International Conference on Computer Vision*, 2023, 6835–6844.
- [15] Qu Z, Jin H, Zhou Y, Yang Z, Zhang W. Focus on local: Detecting lane marker from bottom up via key point. In *Proceedings of the IEEE/CVF Conference on Computer Vision and Pattern Recognition*, 2021, 14122–14130.
- [16] Wang J, Ma Y, Huang S, Hui T, Wang F, Qian C, Zhang T. A Keypoint-based Global Association Network for Lane Detection. In *Proceedings of the IEEE/CVF Conference on Computer Vision and Pattern Recognition*, 2022, 1392–1401.
- [17] Qin Z, Wang H, Li X. Ultra fast structure-aware deep lane detection. In *Computer Vision–ECCV 2020: 16th European Conference, Glasgow, UK, August 23–28, 2020, Proceedings, Part XXIV 16*, 2020, 276–291, doi:10.1007/978-3-030-58586-0-17.
- [18] Xu H, Wang S, Cai X, Zhang W, Liang X, Li Z. Curvelane-nas: Unifying lane-sensitive architecture search and adaptive point blending. In *Computer Vision–ECCV 2020: 16th European Conference, Glasgow, UK, August 23–28, 2020, Proceedings, Part XV 16*, 2020, 689–704, doi:10.1007/978-3-030-58555-6-41.
- [19] Feng Z, Guo S, Tan X, Xu K, Wang M, Ma L. Rethinking Efficient Lane Detection via Curve Modeling. In *Proceedings of the IEEE/CVF Conference on Computer Vision and Pattern Recognition*, 2022, 17062–17070.
- [20] Zheng T, Huang Y, Liu Y, Tang W, Yang Z, Cai D, He X. Clrnet: Cross layer refinement network for lane detection. In *Proceedings of the IEEE/CVF conference on computer vision and pattern recognition*, 2022, 898–907.
- [21] Jin D, Kim D, Kim CS. Recursive Video Lane Detection. In *Proceedings of the IEEE/CVF International Conference on Computer Vision*, 2023, 8473–8482.
- [22] Ren S, He K, Girshick R, Sun J. Faster r-cnn: Towards real-time object detection with region proposal networks. *Advances in neural information processing systems*, 2015, 28.
- [23] Redmon J, Divvala S, Girshick R, Farhadi A. You only look once: Unified, real-time object detection. In *Proceedings of the IEEE conference on computer vision and pattern recognition*, 2016, 779–788.
- [24] Redmon J, Farhadi A. Yolov3: An incremental improvement. *arXiv preprint arXiv:1804.02767*, 2018.
- [25] Duan K, Bai S, Xie L, Qi H, Huang Q, Tian Q. Centernet: Keypoint triplets for object detection. In *Proceedings of the IEEE/CVF international conference on computer vision*, 2019, 6569–6578.
- [26] Tian Z, Shen C, Chen H, He T. Fcos: Fully convolutional one-stage object detection. In *Proceedings of the IEEE/CVF*

international conference on computer vision, 2019, 9627–9636.

[27] Carion N, Massa F, Synnaeve G, Usunier N, Kirillov A, Zagoruyko S. End-to-end object detection with transformers. In *Computer Vision–ECCV 2020: 16th European Conference, Glasgow, UK, August 23–28, 2020, Proceedings, Part I 16*, 2020, 213–229, doi:10.1007/978-3-030-58452-8_13.

[28] Zhu X, Su W, Lu L, Li B, Wang X, Dai J. Deformable detr: Deformable transformers for end-to-end object detection. *arXiv preprint arXiv:2010.04159*, 2020.

[29] Liu S, Li F, Zhang H, Yang X, Qi X, Su H, Zhu J, Zhang L. Dab-detr: Dynamic anchor boxes are better queries for detr. *arXiv preprint arXiv:2201.12329*, 2022.

[30] Kuhn HW. The Hungarian method for the assignment problem. *Naval research logistics quarterly*, 1955, 2(1-2): 83–97.

[31] Liao B, Chen S, Wang X, Cheng T, Zhang Q, Liu W, Huang C. Maptr: Structured modeling and learning for online vectorized hd map construction. *arXiv preprint arXiv:2208.14437*, 2022.

[32] Zhu X, Su W, Lu L, Li B, Wang X, Dai J. Deformable detr: Deformable transformers for end-to-end object detection. *arXiv preprint arXiv:2010.04159*, 2020.

[33] Li F, Zhang H, Liu S, Zhang L, Ni LM, Shum HY, et al.. Mask dino: Towards a unified transformer-based framework for object detection and segmentation. *arXiv preprint arXiv:2206.02777*, 2022.

[34] Lin TY, Maire M, Belongie S, Hays J, Perona P, Ramanan D, Dollár P, Zitnick CL. Microsoft coco: Common objects in context. In *Computer Vision–ECCV 2014: 13th European Conference, Zurich, Switzerland, September 6–12, 2014, Proceedings, Part V 13*, 2014, 740–755, doi: 10.1007/978-3-319-10602-1_48.

Author biography



Zhongyu Yang received his M.S. degree from the University of Electronic Science and Technology of China (UESTC) , Chengdu, in 2023. He is now an algorithm engineer in Didi Chuxing.



Ruini Xue received a Ph.D. degree from Tsinghua University in 2009, and is currently an associate professor with the School of Computer Science and Engineering in UESTC. His research interests include distributed storage systems, graph computing and AI.